

1    **Supplementary Information**

2    **SEEDING to enable sensitive electrochemical detection of**  
3    **biomarkers in undiluted biological samples**

4

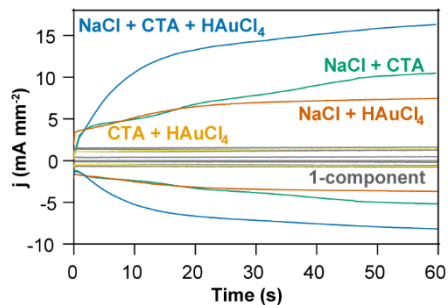
5    *Jonathan Sabaté del Río<sup>1</sup>, Hyun-Kyung Woo<sup>1,2</sup>, Juhee Park<sup>1</sup>, Hong Koo Ha<sup>3</sup>, Jae-*  
6    *Ryong Kim<sup>4</sup>, Yoon-Kyoung Cho<sup>1,2\*</sup>*

7    <sup>1</sup>Center for Soft and Living Matter, Institute for Basic Science (IBS), Ulsan, 44919  
8    Republic of Korea; <sup>2</sup>Department of Biomedical Engineering, Ulsan National Institute  
9    of Science and Technology (UNIST), Ulsan, 44919 Republic of Korea; <sup>3</sup>Department  
10   of Urology, Pusan National University Hospital, Pusan National University School of  
11   Medicine, Busan 49241, Republic of Korea; <sup>4</sup>Department of Biochemistry and  
12   Molecular Biology, Smart-aging Convergence Research Center, College of Medicine,  
13   Yeungnam University, Daegu 42415, Republic of Korea;

14

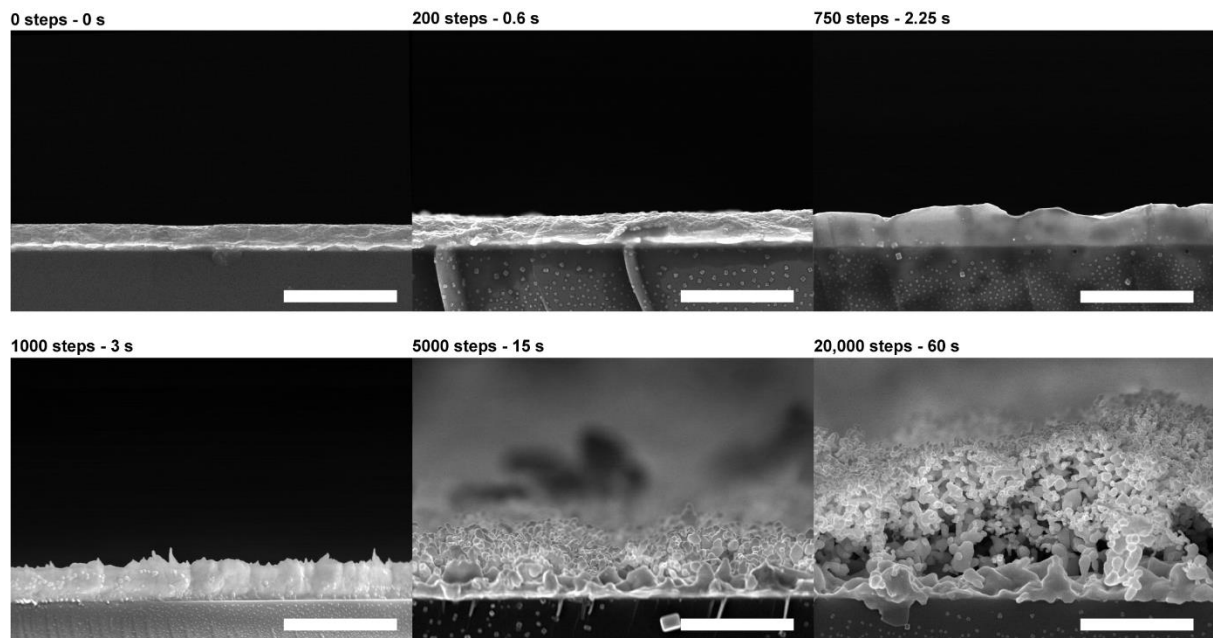
15

16   \*Correspondence to: [ykcho@unist.ac.kr](mailto:ykcho@unist.ac.kr) (Y.-K.C.)



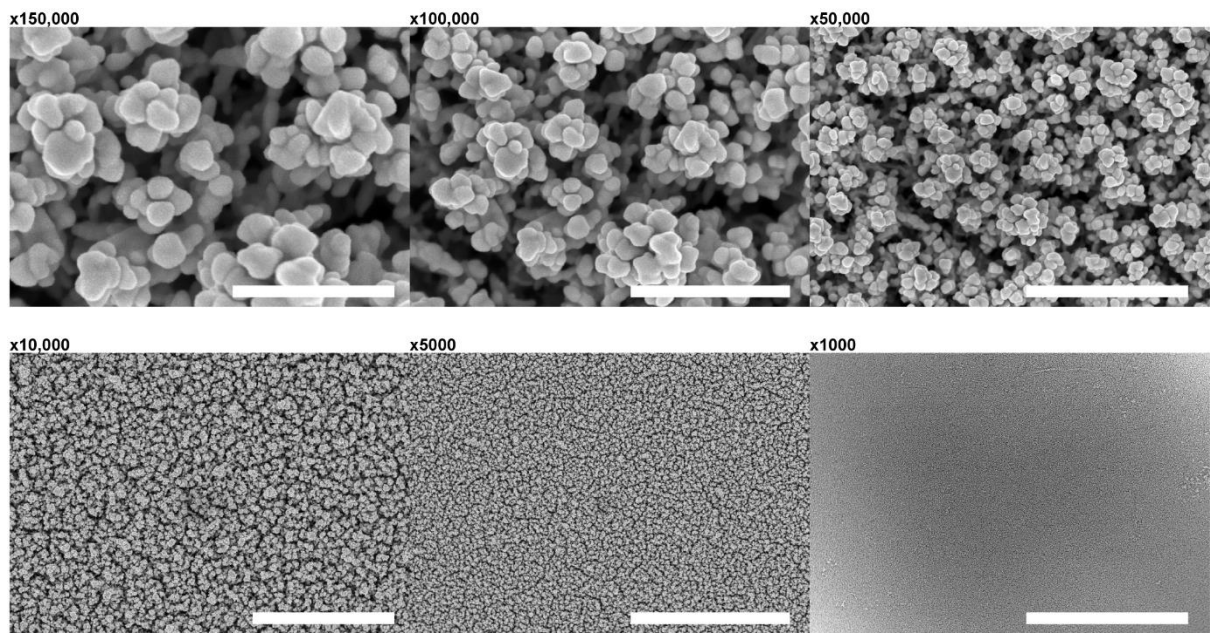
17

18 **Supplementary Fig. 1** | Typical chronoamperograms, showing both cathodic and  
 19 anodic currents, during the nanostructuring process conducted in photolithographic  
 20 gold electrodes in different control solutions (one-component controls are all greyed  
 21 out).

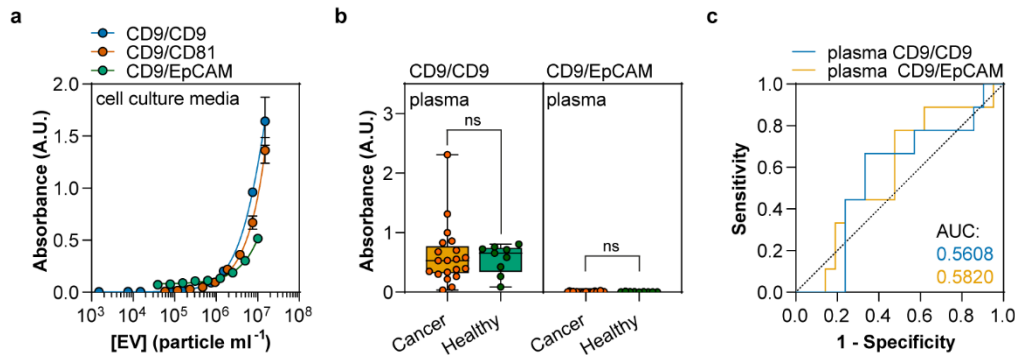


22

23 **Supplementary Fig. 2** | Scanning electron micrographs of cross-sections of  
24 nanostructured gold electrodes conducted by chronoamperometry after different  
25 numbers of voltage steps. Scale bar: 2  $\mu$ m.



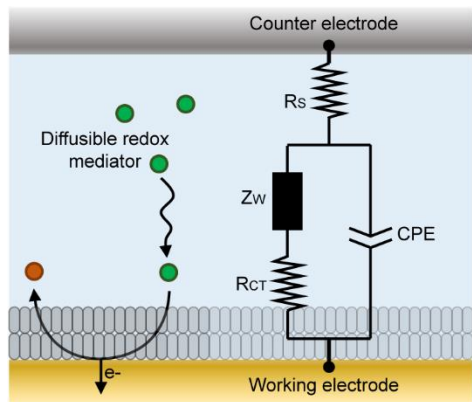
27 **Supplementary Fig. 3 |** Scanning electron micrographs of nanostructured gold  
28 electrodes at different magnifications, displaying grain detail at higher magnifications  
29 and surface homogeneity at low magnifications (scale bars: from left to right, top to  
30 bottom: 300 nm, 500 nm, 1  $\mu$ m, 5  $\mu$ m, 10  $\mu$ m, and 50  $\mu$ m).



31

32 **Supplementary Fig. 4 |** Calibration plot for detection of CD9<sup>+</sup>, CD81<sup>+</sup> or EpCAM<sup>+</sup> on  
 33 CD9-captured extracellular vesicles from cell culture media, representing  
 34 absorbance (circles) vs. particle concentration in traditional ELISA (n = 4 wells). Error  
 35 bars represent the standard deviation of the mean. **b**, Analysis of clinical human  
 36 plasma samples using ELISA with different assay schemes, detection of CD9<sup>+</sup> or  
 37 EpCAM<sup>+</sup> on CD9-captured extracellular vesicles (21 cancer samples and nine  
 38 healthy samples with three technical replicates for each). The boxes extend from the  
 39 25<sup>th</sup> to 75<sup>th</sup> percentiles, the middle line is the median, and the whiskers extend from  
 40 min to max values. **c**, Characteristic curve showing the classification ability (healthy,  
 41 cancer) for the two employed assays on plasma clinical samples.

42



43 **Supplementary Fig. 5 |** Nyquist equivalent circuit and schematic representation of  
44 each element of the circuit.

45 **Supplementary table 1. Facet relative abundance in flat and NSG electrodes**

Sample	Facet relative abundance (%)				Crystallite size (nm)
	(111)	(200)	(220)	(311)	
Flat gold	13	10	72	5	19 ± 4
NSG	17	12	63	8	21 ± 4

46 **NSG:** Nanostructured and nanoporous gold

**Supplementary table 2. Other methods to generate high surface gold electrodes.**

Method	Suitable for Photo-lithographic electrodes?	Acids, Toxic reagents or Solvents?	Fabrication throughput	Complexity	Time	Residues	Porosity / anti-biofouling	Ref.
EC etching	✗	✓	•	••	•••	✗	✓	1, 2
Template-free ED	✓	✗	••	••	•	✗	✗	3
Nanoporous filter template ED	✓	✓	•	•••	••	✗	✓	4, 5
Surfactant-based template ED	✓	✓	••	•••	••	✗	✗	6
EC roughening	✗	✓	••	•	•	✗	✗	7
Nanoparticles	✓	✗	••	•	•	✗	✗	8
PVD + chemical dealloying	✓	✓	•••	•••	•••	✓	✓	9
EC dealloying	✓	✓	•••	•••	•••	✗	✓	10
ED and EC dealloying	✗	✓	•	••	••	✓	✓	11
SEEDING	✓	✗	••	••	•	✗	✓	

**EC:** Electrochemical, **ED:** Electrodeposition, **PVD:** Physical vapor deposition (thermal evaporation or sputtering)

X: No, ✓: Yes, •: Low, ••: Middle, •••: High. The symbols are colored in green when the outcome is good/positive, red when is bad/negative, and grey when is fair.

## Supplementary References

1. Sukeri, A., Saravia, L. P. H., Bertotti, M. A facile electrochemical approach to fabricate a nanoporous gold film electrode and its electrocatalytic activity towards dissolved oxygen reduction. *Phys. Chem. Chem. Phys.* **17**, 28510-28514 (2015).
2. Deng, Y., Huang, W., Chen, X., Li, Z. Facile fabrication of nanoporous gold film electrodes. *Electrochem. commun.* **10**, 810-813 (2008).
3. Soleymani, L., Fang, Z., Sargent, E. H., Kelley, S. O. Programming the detection limits of biosensors through controlled nanostructuring. *Nat. Nanotechnol.* **4**, 844 (2009).
4. Zhang, X., Li, D., Bourgeois, L., Wang, H., Webley, P. A. Direct electrodeposition of porous gold nanowire arrays for biosensing applications. *Chemphyschem.* **10**, 436-441 (2009).
5. Bahari Mollamahale, Y., Ghorbani, M., Dolati, A., Hosseini, D. Electrodeposition of well-defined gold nanowires with uniform ends for developing 3D nanoelectrode ensembles with enhanced sensitivity. *Mater. Chem. Phys.* **213**, 67-75 (2018).
6. Lim, H., *et al.* A universal approach for the synthesis of mesoporous gold, palladium and platinum films for applications in electrocatalysis. *Nat. Protoc.* **15**, 2980-3008 (2020).
7. Arroyo-Currás, N., Scida, K., Ploense, K. L., Kippin, T. E., Plaxco, K. W. High Surface Area Electrodes Generated via Electrochemical Roughening Improve the Signaling of Electrochemical Aptamer-Based Biosensors. *Anal. Chem.* **89**, 12185-12191 (2017).
8. Young, S. L., Kellon, J. E., Hutchison, J. E. Small Gold Nanoparticles Interfaced to Electrodes through Molecular Linkers: A Platform to Enhance Electron Transfer and Increase Electrochemically Active Surface Area. *J. Am. Chem. Soc.* **138**, 13975-13984 (2016).
9. Rouya, E., Cattarin, S., Reed, M. L., Kelly, R. G., Zangari, G. Electrochemical Characterization of the Surface Area of Nanoporous Gold Films. *J. Electrochem. Soc.* **159**, K97-K102 (2012).
10. Lackmann, A., Baumer, M., Wittstock, G., Wittstock, A. Independent control over residual silver content of nanoporous gold by galvanodynamically controlled dealloying. *Nanoscale.* **10**, 17166-17173 (2018).

11. Jia, F., Yu, C., Ai, Z., Zhang, L. Fabrication of Nanoporous Gold Film Electrodes with Ultrahigh Surface Area and Electrochemical Activity. *Chem. Mater.* **19**, 3648-3653 (2007).